中国地震局地震研究所
Institute of Seismology, China Earthquake Administration

Workshop of Jinping Neutrino Experiment 2026

Preliminary Analysis and Discussion on Subsurface Density and Thermal Structure of the China Jinping Underground Laboratory and Its Surrounding Region

Presenter: Ren Yuxuan (Master Student)

Supervisors: Xi Yufei, Wu Guiju

Institute of Seismology, China Earthquake Administration

Institute of Hydrogeology and Environmental Geology, Chinese Academy of Geological Sciences

July 2, 2026 (Xichang)

CONTENTS

- Background
- Data Sources and Methods
- Results and Discussion
- Prospects

Background

❖ Regional Tectonic Setting

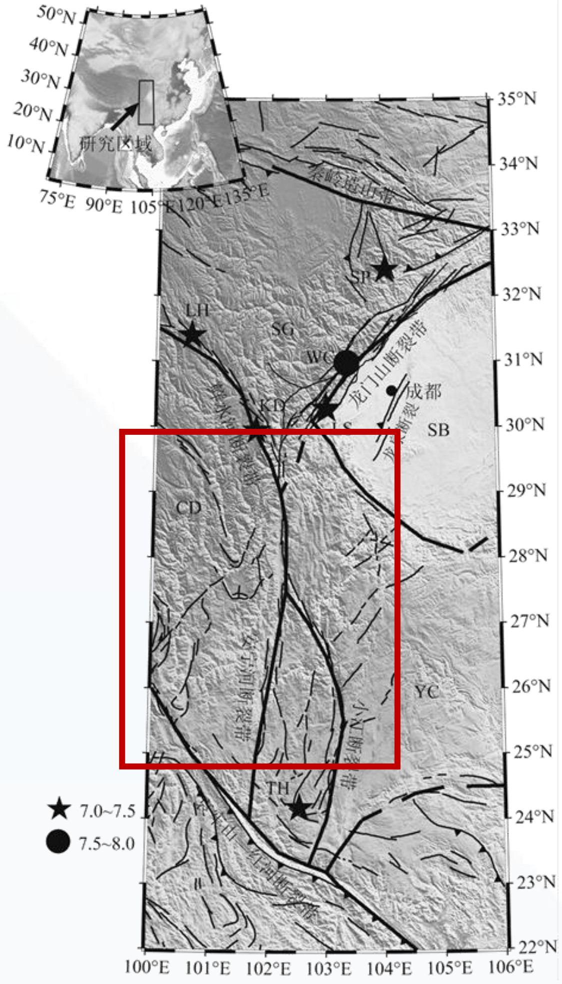

North-South Seismic Belt (Hu et al., 2017)

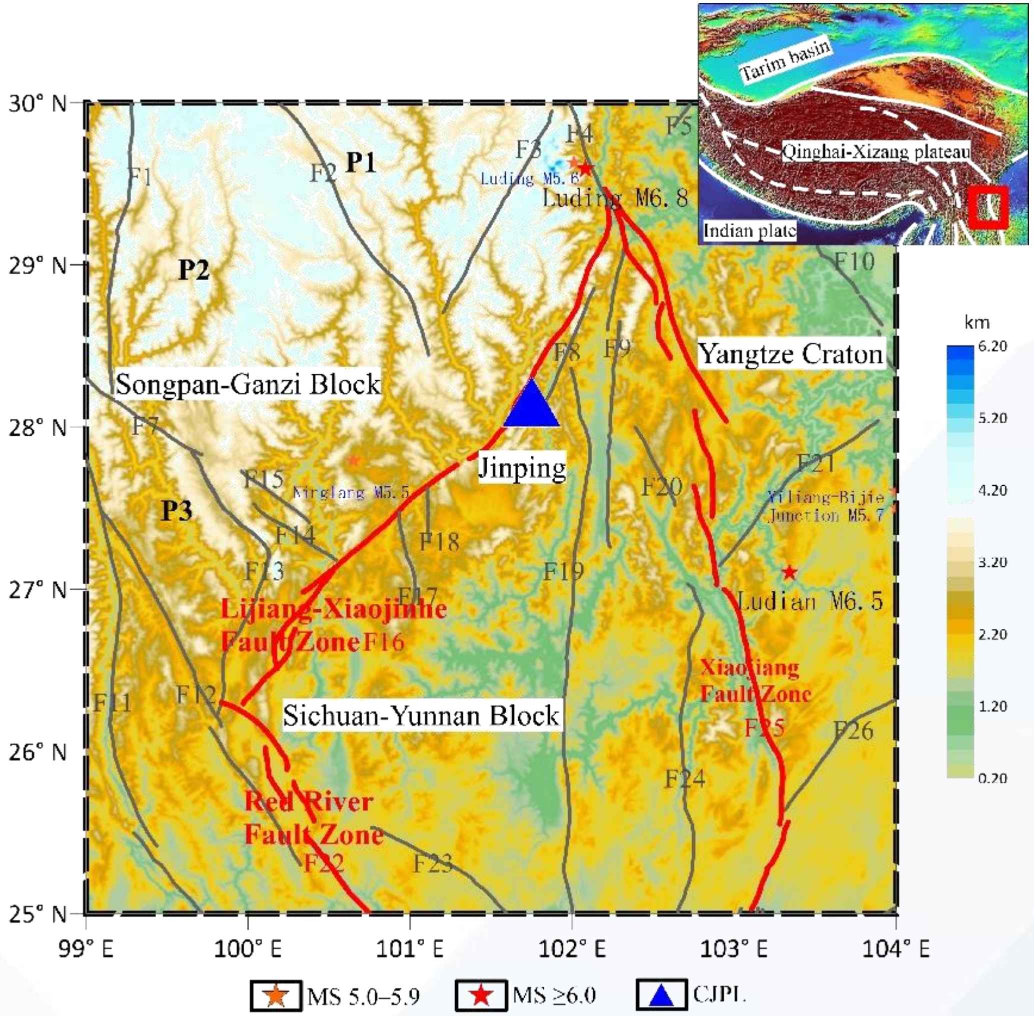

Topographic Map of the Study Area

- **Plate Subduction and Deep Mantle Structure**
- **North-South Seismic Belt**
- **Two Mainstream Tectonic Models**
  - Rigid Block Extrusion Model
  - Lower Crustal Flow Model

Background

❖ Regional Tectonic Setting

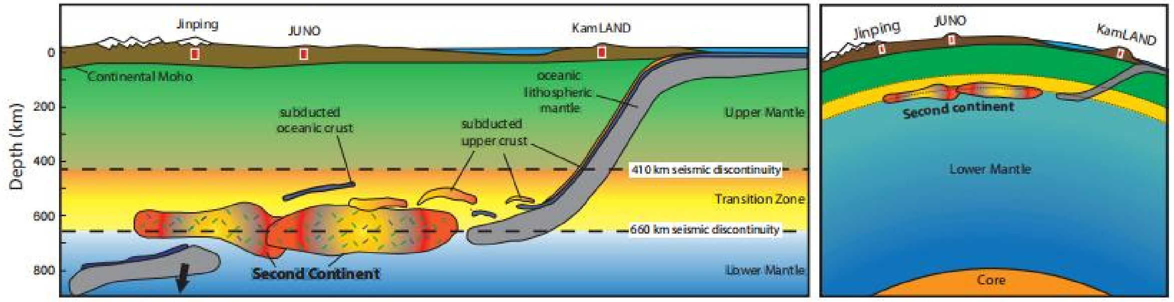

Figure 1. Left panel shows cartoon illustration of a second continent that formed under eastern China due to Pacific-type subduction occurring along the western margin of the Pacific basin. Picture is an adaptation of Fig. 5. in [*Kawai et al.*, 2013]. The proximity of 3 geoneutrino experiments to this putative second continent are shown as being underground in Japan (KamLAND) and China (JUNO and Jinping). These 3 detectors see approximately the same mantle volume and similar global crust, see right panel, which results in a major reduction in the predicted uncertainties. Local differences in the geoenutrino fluxes for each of these detectors are due to geological differences in the nearby lithosphere (closest 500 km) surrounding the detector; this region contributes approximately half of the detected signal.

Schematic Diagram of the Second Continent Hypothesis (Roskovec et al., 2018)

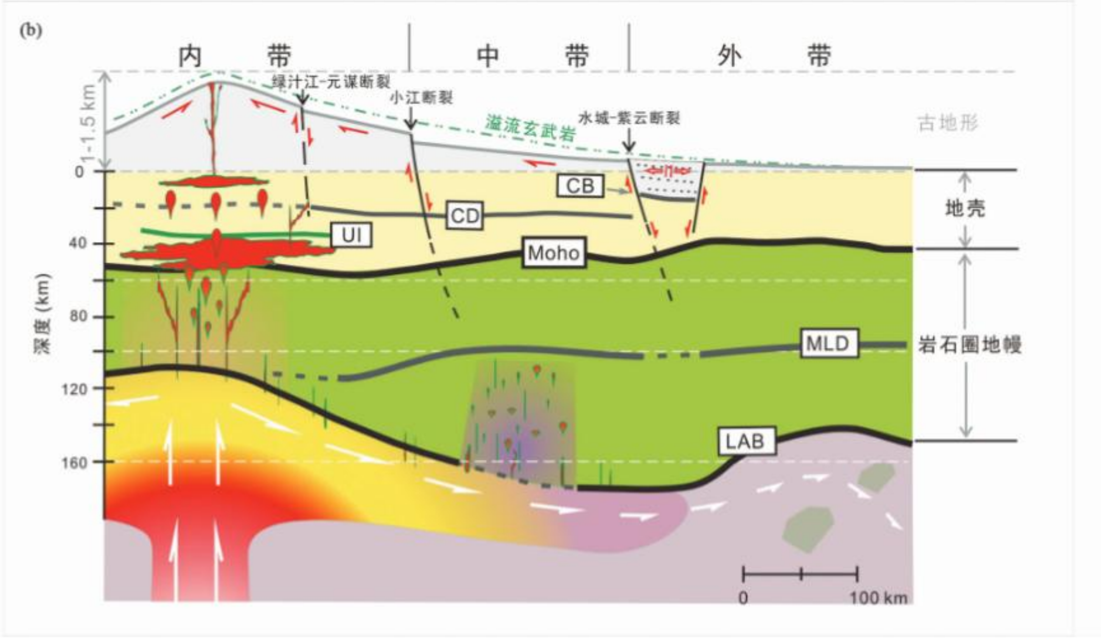

图 5 峨眉山大火成岩省岩石圈几何结构及地幔柱-岩石圈相互作用解释图(据徐义刚等, 2017 修改)
(a)峨眉山大火成岩省岩石圈结构的主要特征,其中壳内结构基于 COMPASS-ELIP 剖面远震 *P* 波接收函数成像获得(Chen *et al.*, 2015),岩石圈地幔结构基于本文远震 *S* 波接收函数成像获得;(b)根据岩石圈结构特征进行地质解释,获得的二叠纪地幔柱-岩石圈相互示意图. 其中,UI 为高速下地壳指示的岩浆底侵层顶界面,CD 为康拉德不连续面(上地壳底界面),CB 为水城-紫云裂陷槽沉积层底界面. 除估算的古地形隆升幅度外,岩石圈内部主要界面均从接收函数成像结果提取并按比例尺显示

Schematic Diagram of Mantle Plume Upwelling and Emeishan Large Igneous Province (Chen et al., 2023)

- ➢ **The Second Continent and Deep Material Circulation**
- ➢ **Mantle Plume Upwelling and Emeishan Large Igneous Province**

Background

❖ Regional Tectonic

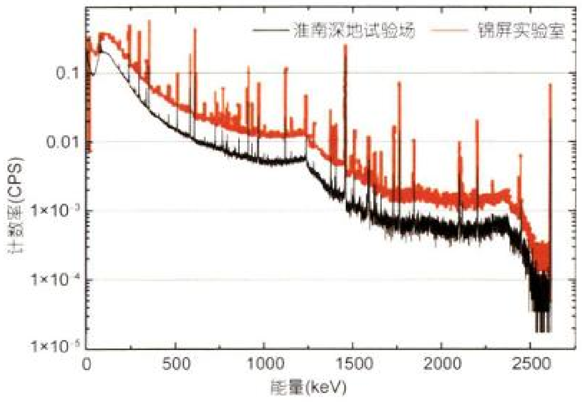

图 4 淮南潘一东煤矿井下与锦屏实验室γ能谱测量结果

锦屏实验室γ能谱数据来自Zeng等(2014)

钾等的含量进行了采样和分析测试(黄文辉等，2001；王永利等，2004；刘强等，2018)．如表3所示锦屏与淮南煤岩的放射性元素含量对比，显然二者均处于同一水平，锦屏因围岩为海相碳酸盐岩和大理岩而呈现相对较低的水平．

2.2.2 重力观测

本次重力观测所用两种重力仪均属于弹簧重力仪，侧重于重力噪声水平评价．地下巷道内有风机、水泵、升降罐笼、变压器、高压输电线路、铁轨等多个可能的噪声干扰源，对大于mHz的高频重力信号噪声水平可能有影响．

图5是地表与海拔−848m巷道的原始重力观测数

表 3 淮南煤岩与锦屏大理岩U/Th/K含量对比[a)]

地点	U-238(Bq kg^{-1})	Th-232(Bq kg^{-1})	K-40(Bq kg^{-1})
锦屏	3.69~4.21	0.52~0.64	4.28
淮南	2.21~14.892	6.84~14.652	6.252

a) 锦屏数据来自于王永利等(2004)

(Wang et al., 2023)

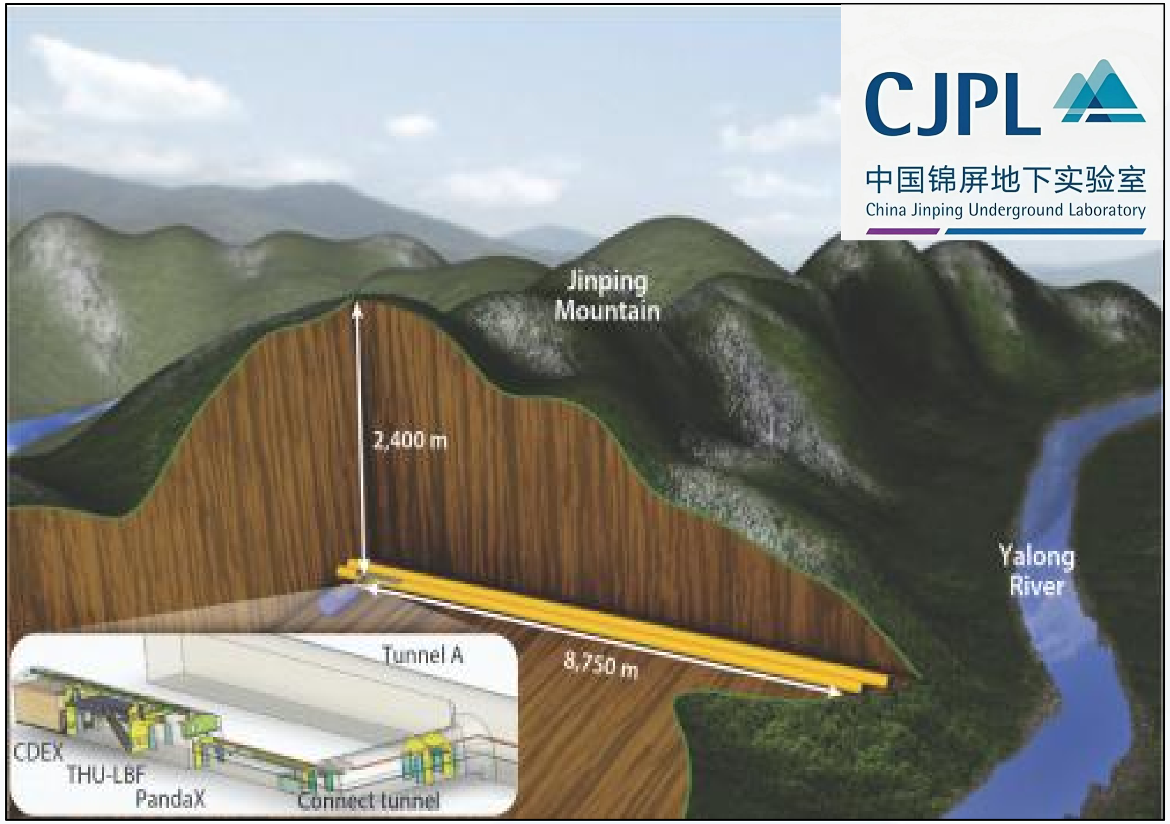

Schematic Diagram of China Jinping Underground Laboratory

➢ **Distribution of Uranium and Thorium and Radiogenic Heat Production**

➢ **China Jinping Underground Laboratory**

Data Sources and Methods

❖ Data Sources

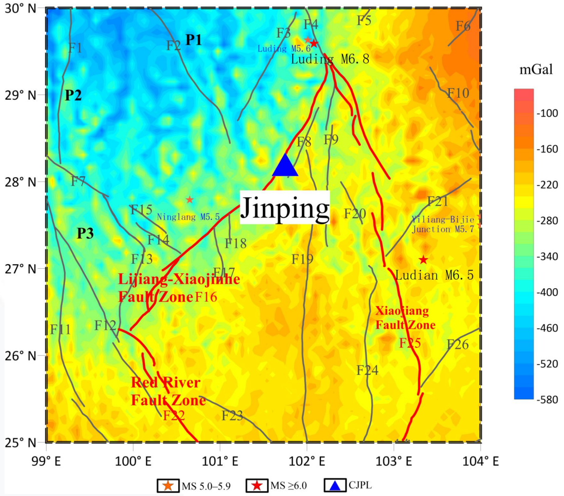

Bouguer Gravity Anomaly

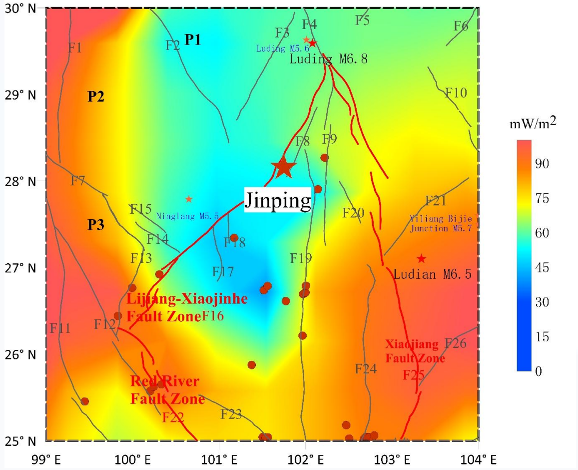

Terrestrial Heat Flow Distribution

Data	Source
Bouguer Gravity Anomaly	WGM2012 (World Gravity Map 2012)
Vs Model	CSRM1.0 (China Seismic Regional Model 1.0)
Thermophysical Parameters	Relevant published studies and reference literature
LAB Depth	LithoRef18 Global Reference Model of the Lithosphere and Upper Mantle
Heat Flow Data	Compilation of Heat Flow Data in the Continental Area of China (5th Edition)
Global Heat Flow Model	The First 0.2° Resolution Global Continental Heat Flow Map: Advancing Fine-Scale Geothermal Modeling
Active Faults	CAFDv2023 (China Active Fault Database Version 2023)

Data Sources and Methods

❖ Flowchart

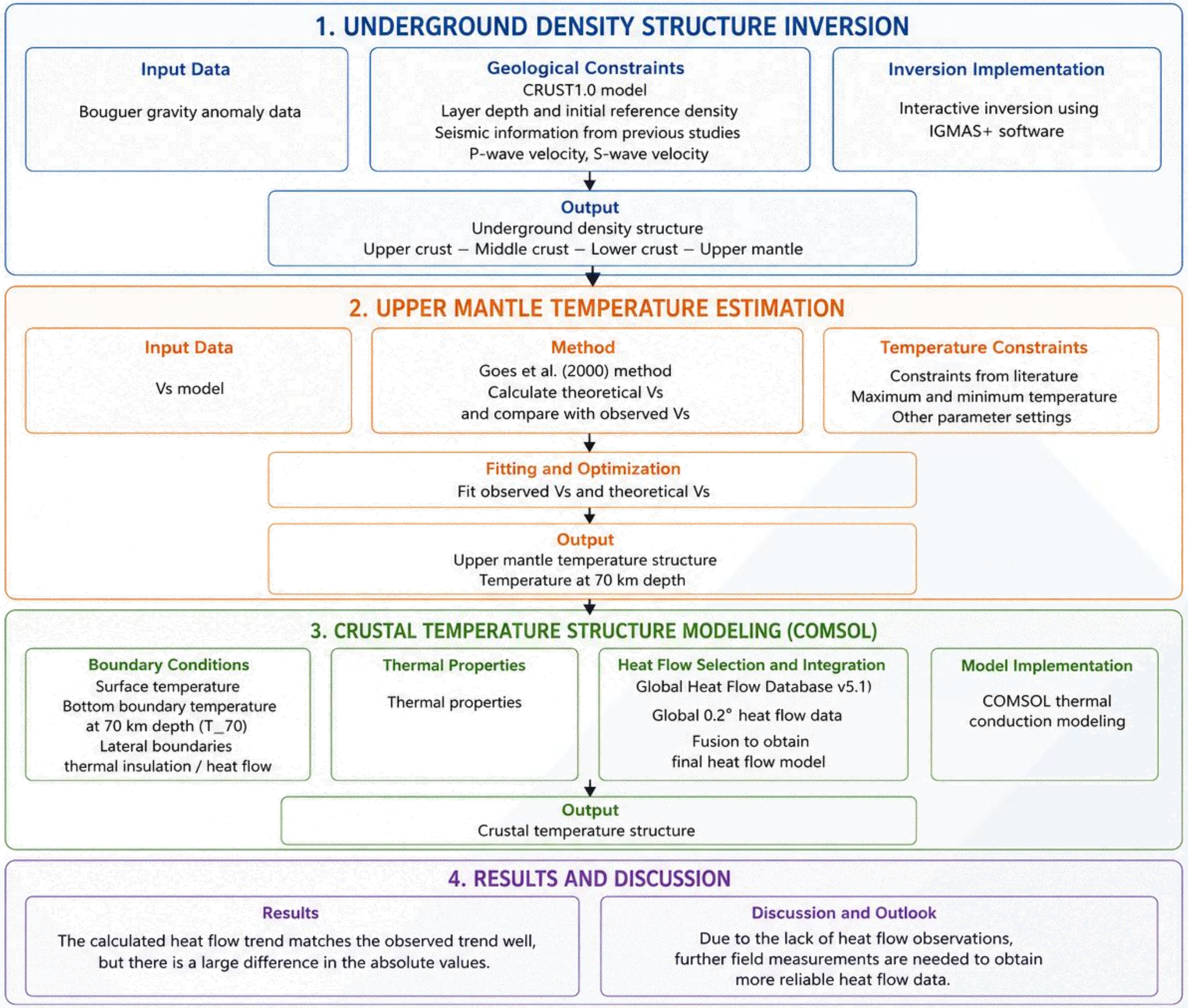

❖ Methods and Principles of Density Inversion

➢ Model Discretization

Let the total number of model cells be N and the number of observation points be M. The gravity anomaly induced by the j-th cell at the i-th observation point is expressed as:

$$\Delta g_{ij} = G_{ij}\rho_j$$

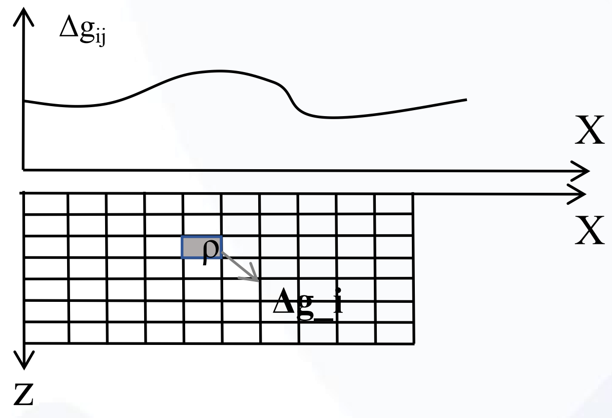

Figure 2. Schematic model of apparent density imaging.

➢ Forward Model

$$\Delta g_i = \sum_{j=1}^{N} G_{ij}\rho_j$$

Δg is an $M \times 1$ vector of observed gravity anomalies, ρ is an $N \times 1$ density vector, G is an $M \times N$ kernel matrix whose elements, G_{ij} are controlled by cell geometric parameters and observation coordinates.

➢ Inversion Method

Preconditioned Conjugate Gradient, PCG

The objective function is defined as:

$$\phi(\rho) = \frac{1}{2}\rho^T A\rho - b^T\rho$$

To reduce the condition number of the coefficient matrix, a preconditioner matrix $P \approx (G^T G)^{-1}$ is introduced to construct the preconditioned system of equations:

$$PG^T G\rho = PG^T \Delta g$$

Data Sources and Methods

❖ Inversion of Upper Mantle Temperature

➢ Core Inversion Method

$$T_{n+1} = T_n + F_{damp} \frac{V_{sobs} - V_{ssyn}(Tn)}{(\partial V_s/\partial T)_{syn}(Tn)}$$

- Inputs: Vs_obs、mineral composition, Q-model parameters
- Output: Equilibrium temperature field

Flowchart for Calculating Upper Mantle Temperature

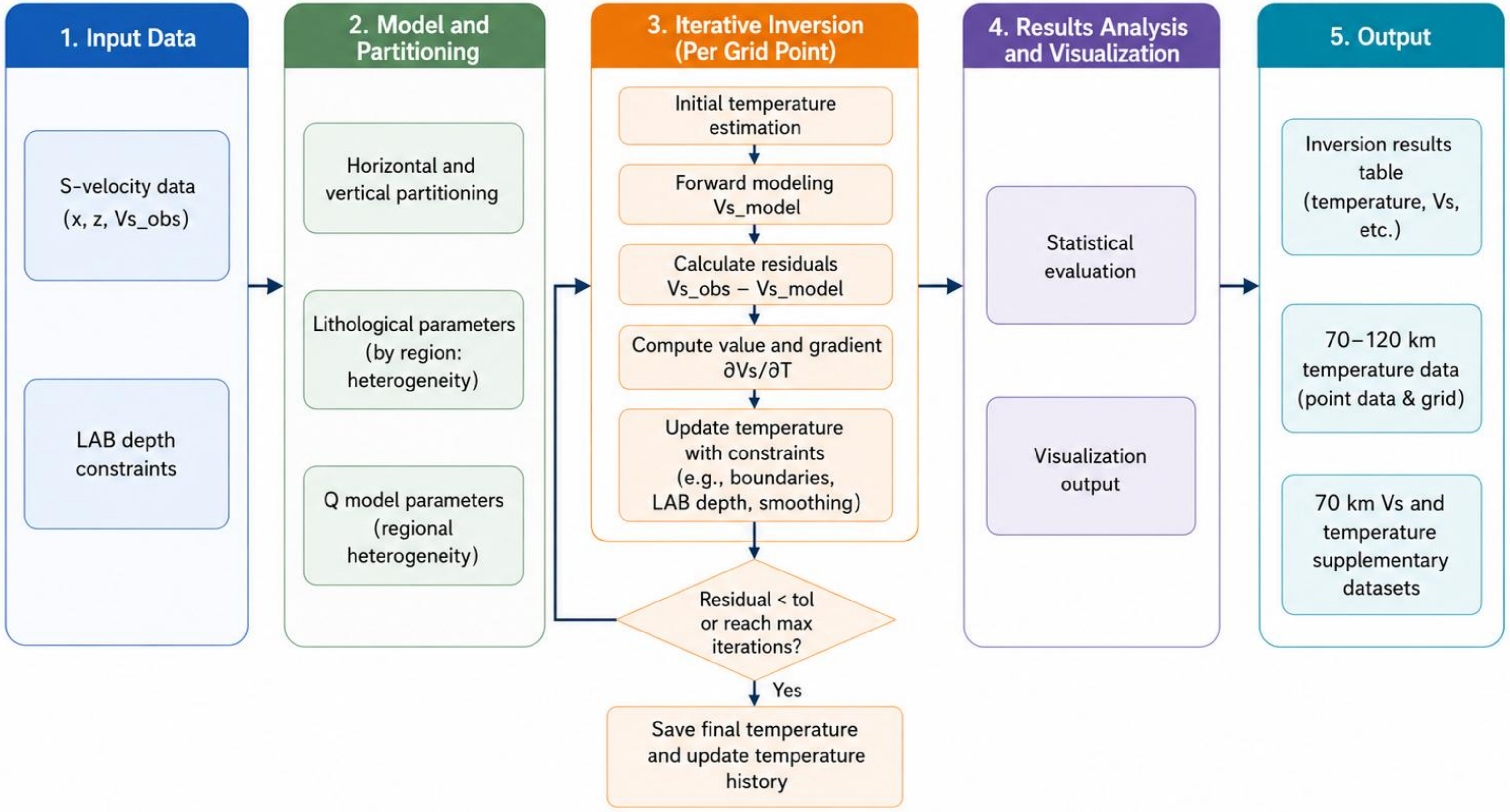

❖ Calculation of Crustal Temperature

Mean Surface Temperature of the Study Area

Thermally Insulated

Heat conduction

Thermally Insulated

Bottom boundary temperature obtained via numerical calculation

- Core Equations

$$d_z\rho C_p \boldsymbol{u}\cdot\nabla T + \nabla\cdot\boldsymbol{q} = d_zQ + q_0 + d_zQ_{\mathrm{ted}}$$

$$\boldsymbol{q} = -d_zk\nabla T$$

- Steady-State Simplification
  - Fluid advection neglected $u=0$
  - Frictional heat generation neglected $Q_{ted}=0$

$$-\nabla\cdot\left(d_zk\nabla T\right) = d_zQ + q_0$$

Results and Discussion

❖ Results of Field-Measured Gravity Data

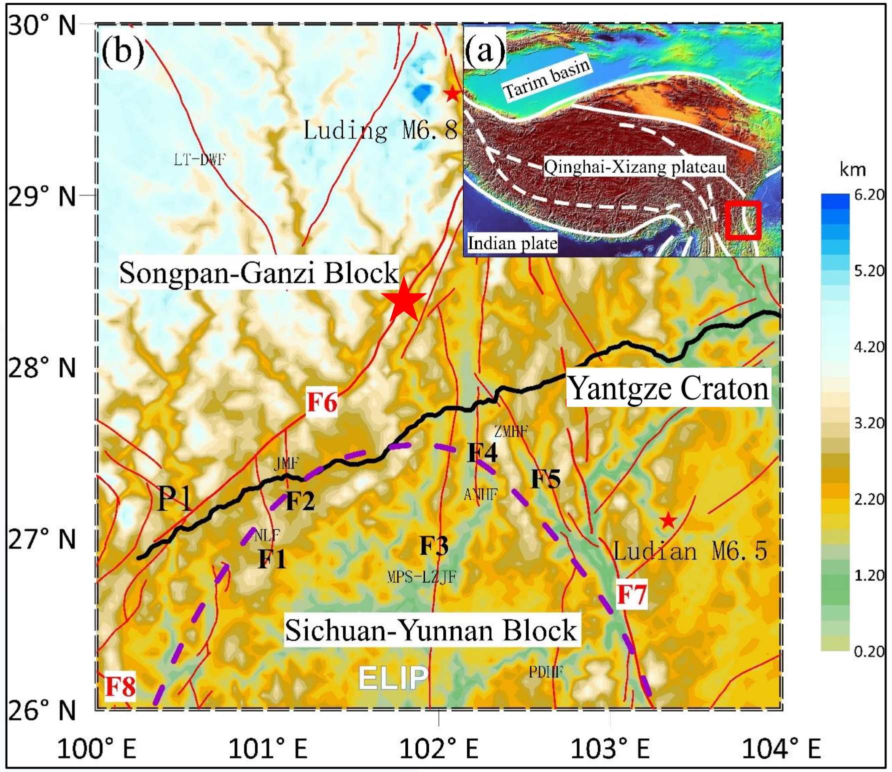

Schematic Diagram Showing Profile Locations of Field Gravity Data

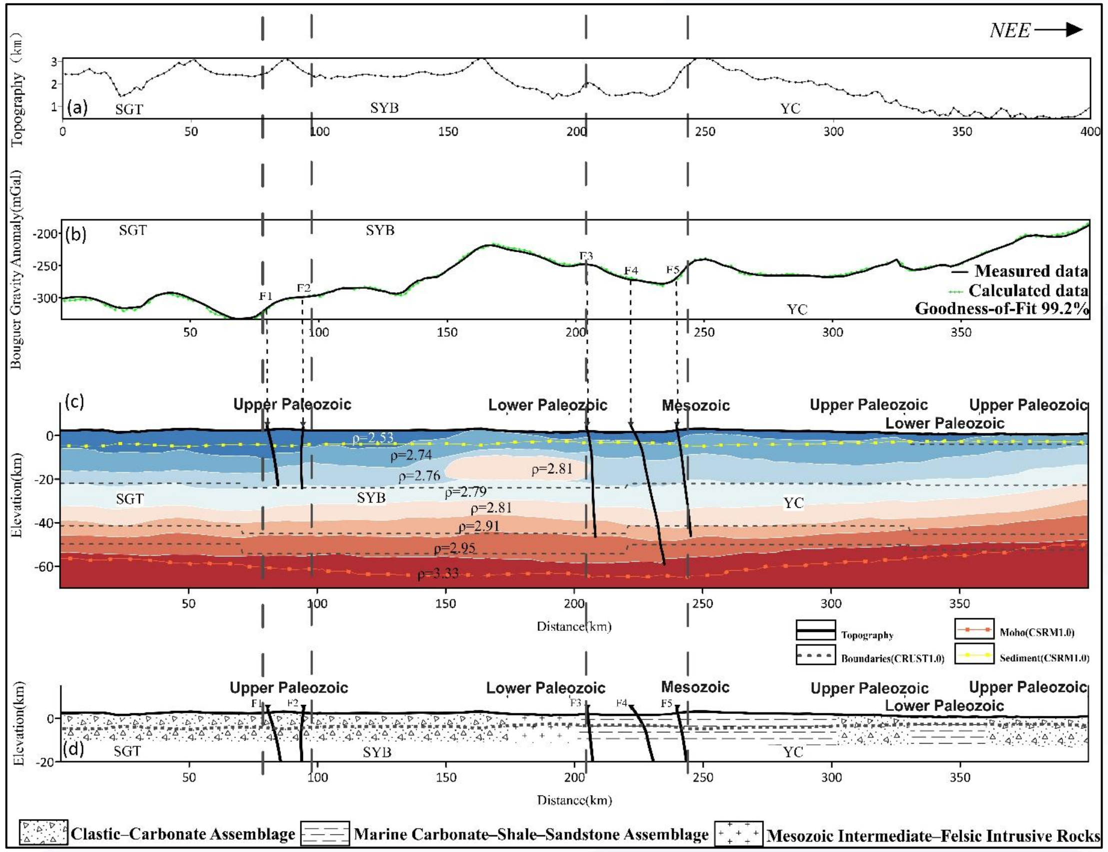

Density Stratification Information Diagram of Field Gravity Data Profiles

- **The terrain is high in the west and low in the east, while the Bouguer gravity anomaly presents a low-west and high-east pattern. The observed Bouguer gravity anomaly values fluctuate drastically, indicating frequent tectonic activities within the study area.**

Results and Discussion

❖ Results of Field-Measured Gravity Data

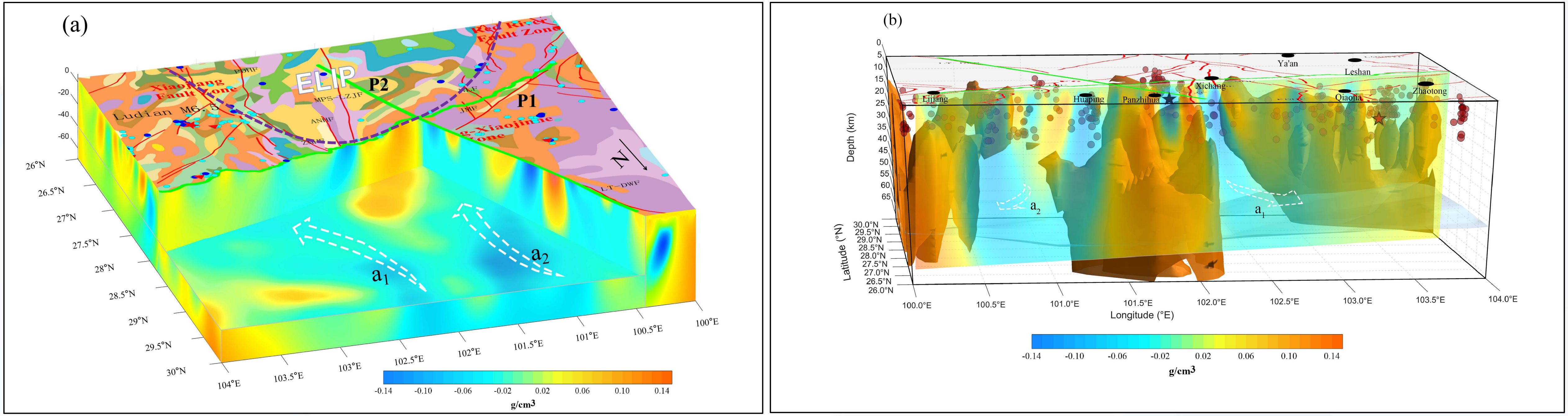

3D Schematic Diagram of Residual Density Anomaly Distribution in the Study Area (submitted Journal of Earth System Science)

- **High-density bodies correspond to the Emeishan Large Igneous Province, while low-density bodies a1 and a2 correspond to the eastern lower crustal flow and western lower crustal flow, respectively.**
- **Blocked by the Emeishan Large Igneous Province, the lower crustal flow migrates toward the southwest and southeast separately.**

Results and Discussion

❖ Density Inversion of Profiles

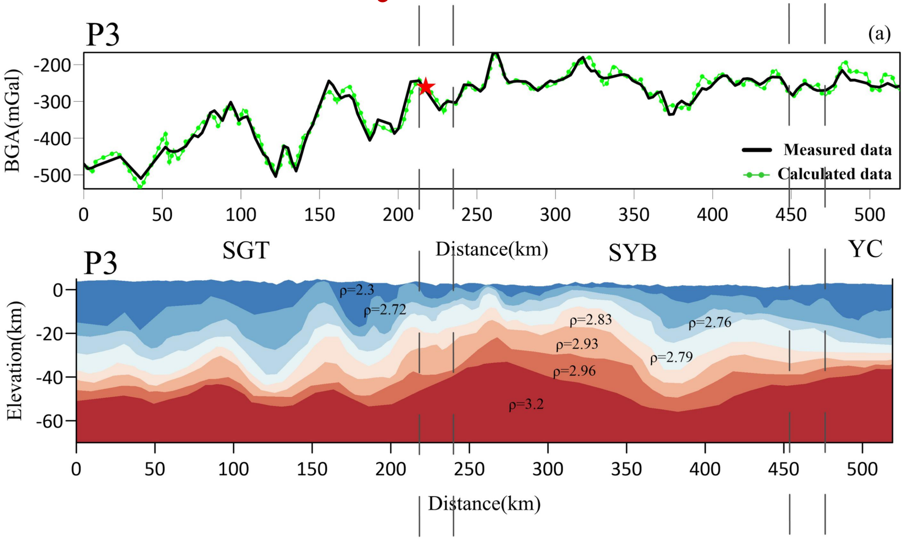

Density Stratification Diagram of Profile P3

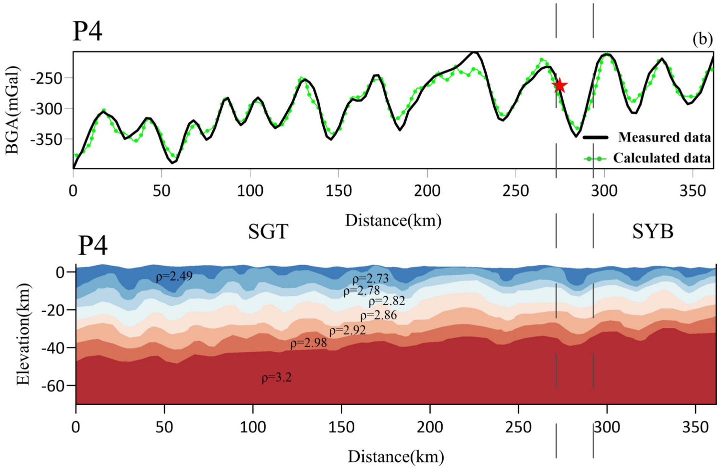

Density Stratification Diagram of Profile P4

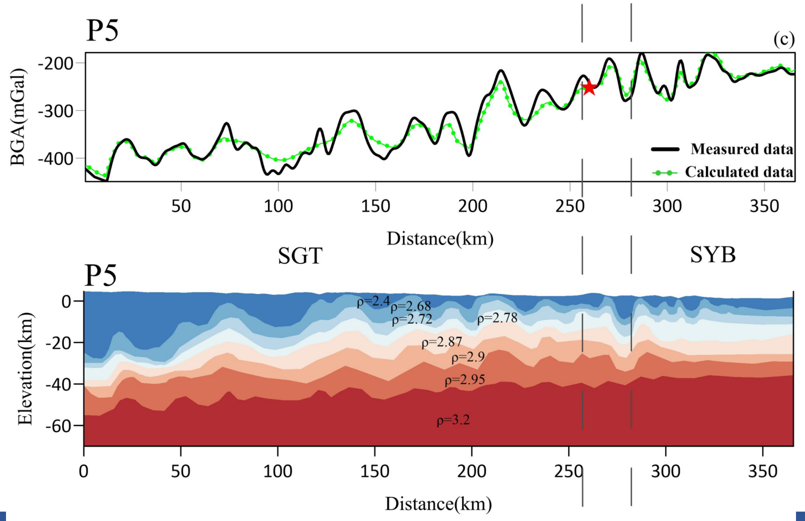

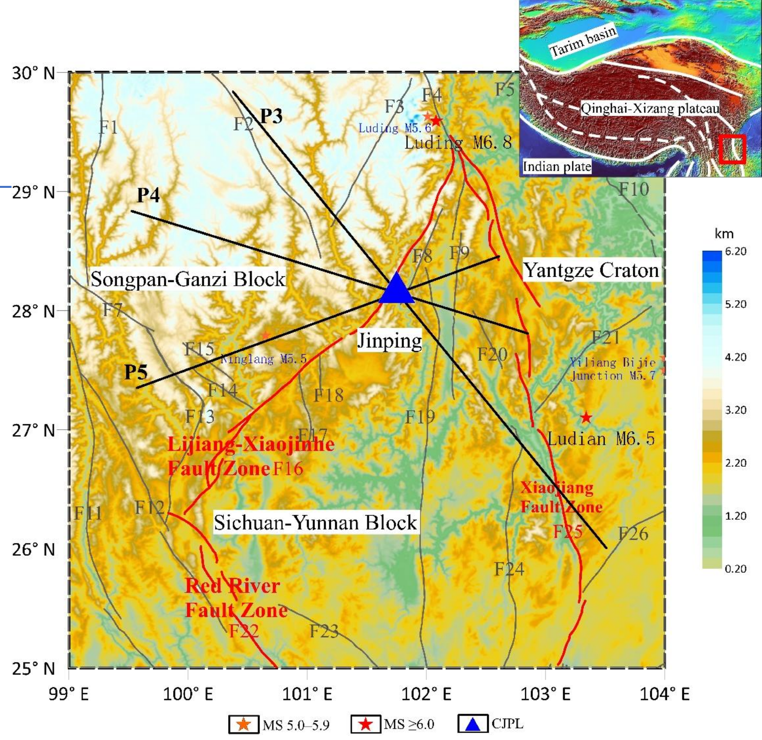

Schematic Diagram of Profile Locations

Stratigraphic Layer	P3(g/cm³)	P4(g/cm³)	P5(g/cm³)
Sedimentary Layer	2.3	2.49	2.4
Upper Crust 1	2.72	2.73	2.68
Upper Crust 2	2.76	2.78	2.72
Middle Crust 1	2.79	2.82	2.78
Middle Crust2	2.83	2.86	2.87
Lower Crust 1	2.93	2.92	2.9
Lower Crust 2	2.96	2.98	2.95
Upper Mantle	3.2	3.2	3.2

Density Stratification Diagram of Profile P5

Results and Discussion

❖ Upper Mantle Temperature (P3)

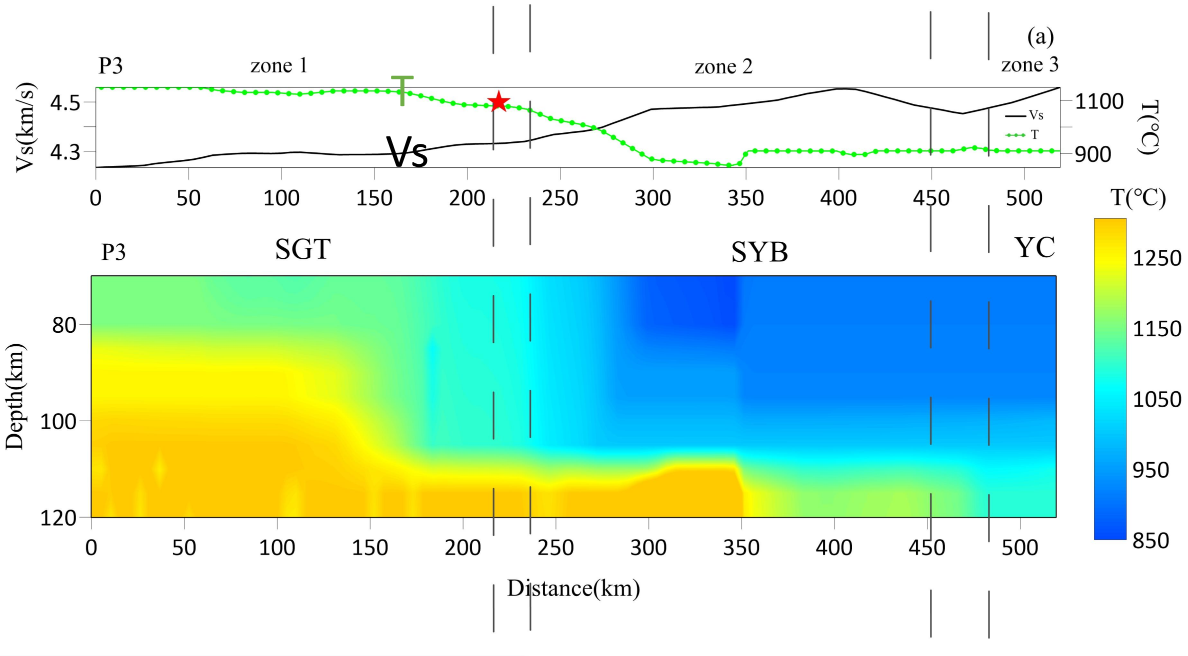

Upper Mantle Temperature along Profile P3

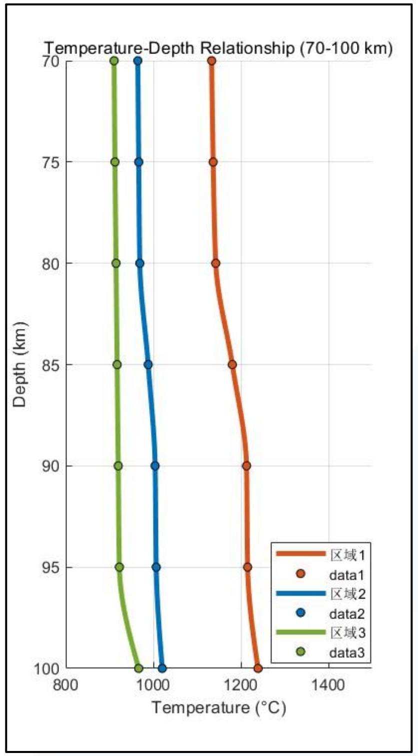

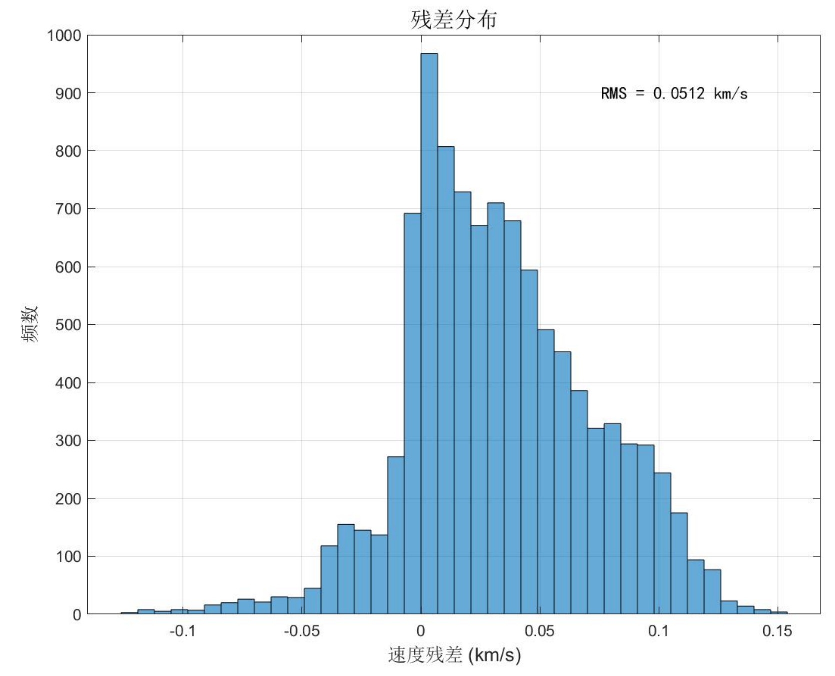

❖ Upper Mantle Temperature (P4)

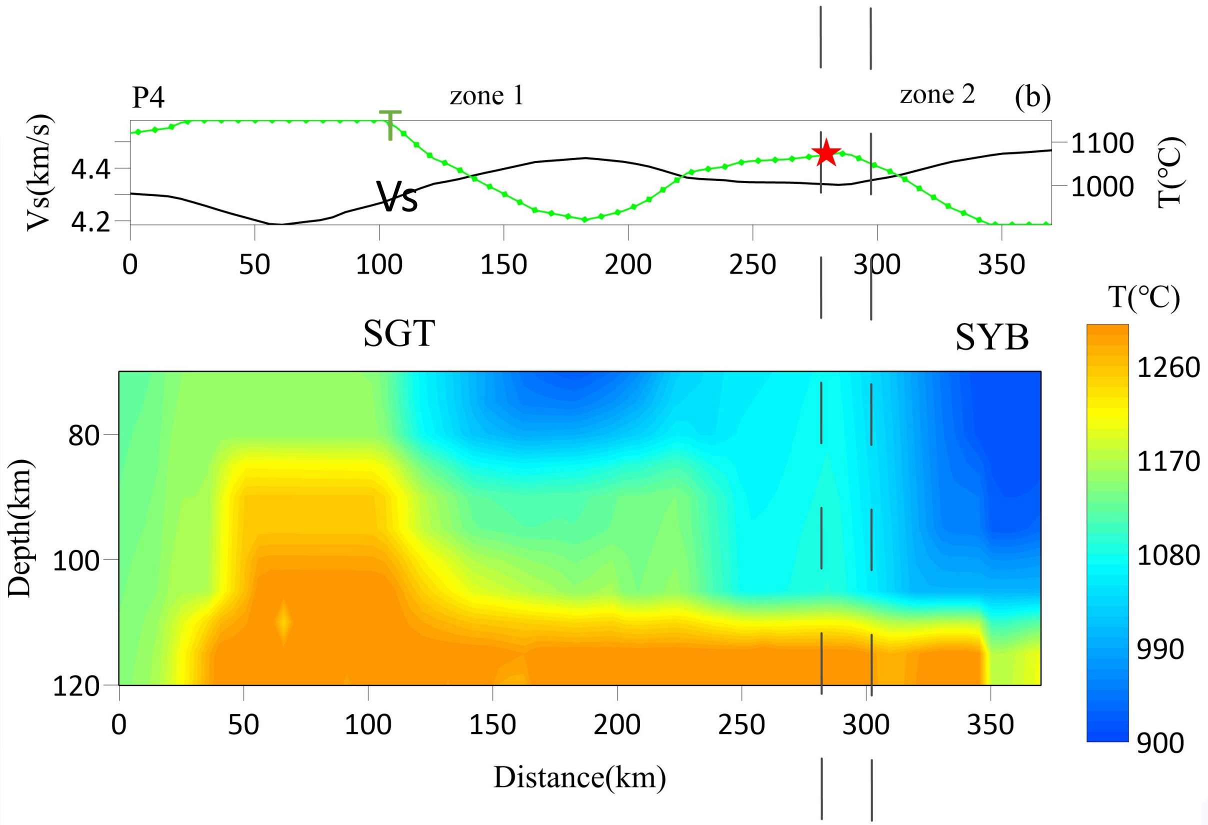

Upper Mantle Temperature along Profile P4

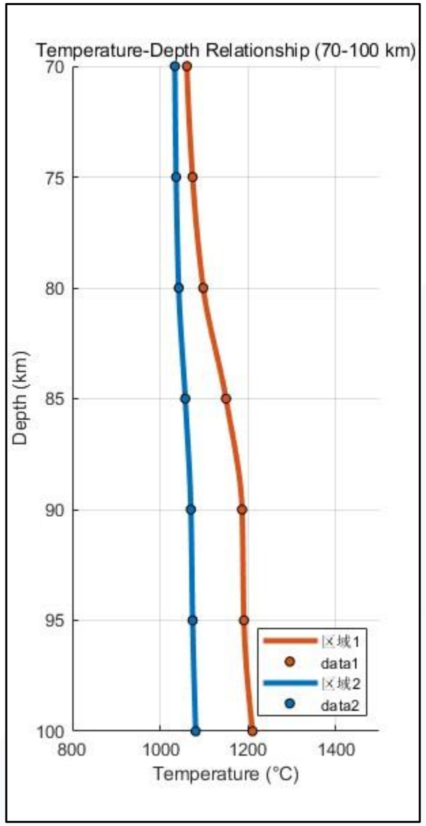

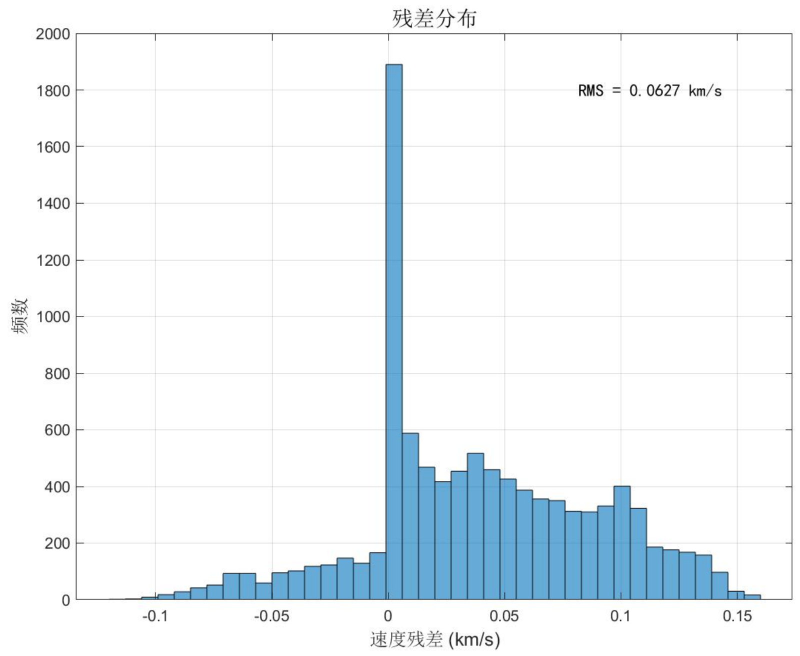

❖ Upper Mantle Temperature (P5)

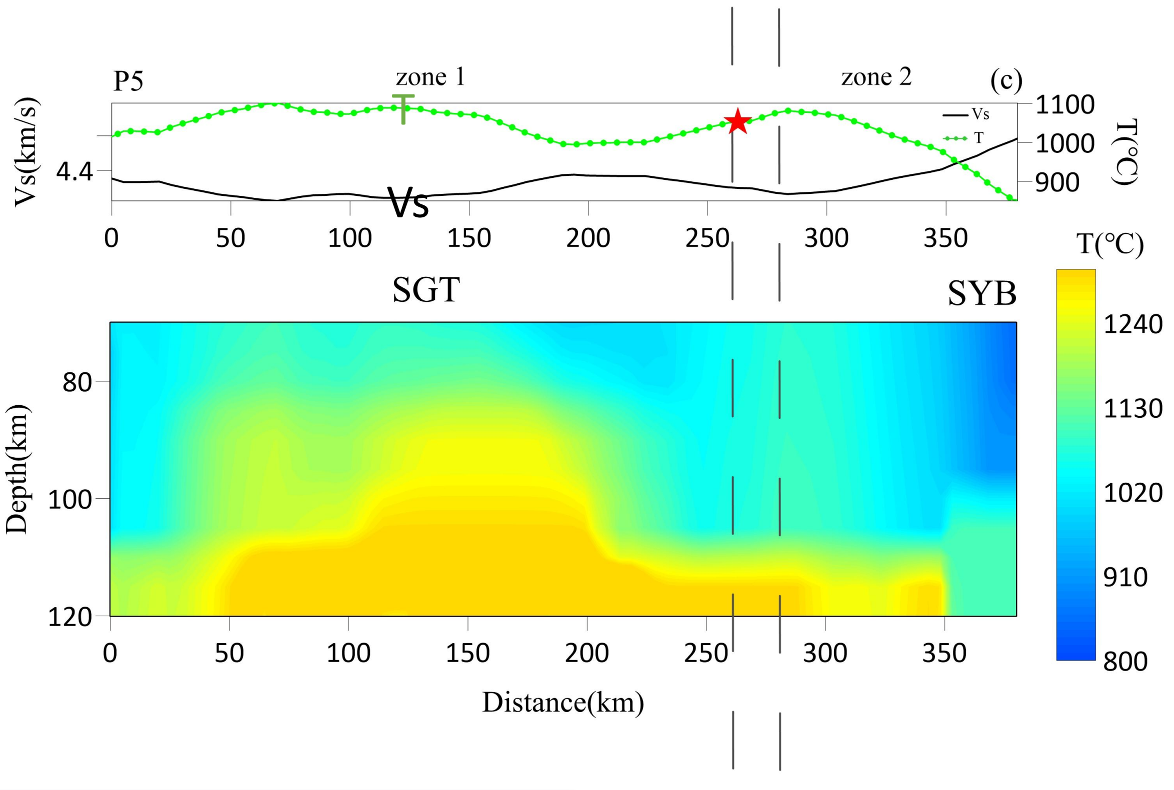

Upper Mantle Temperature along Profile P5

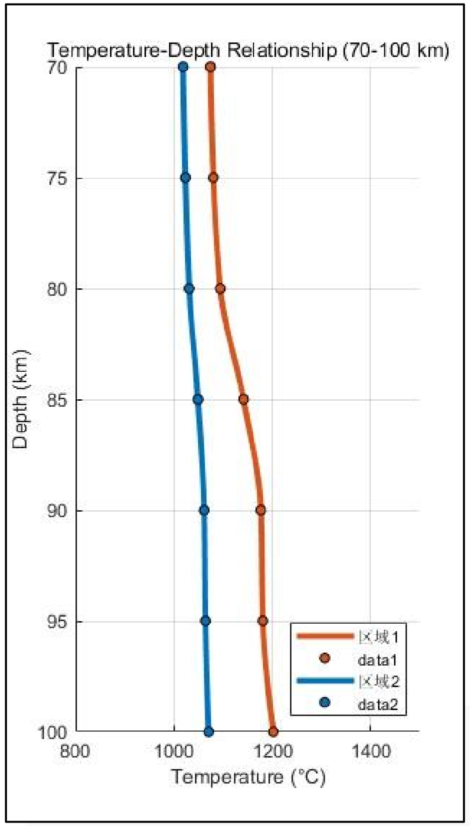

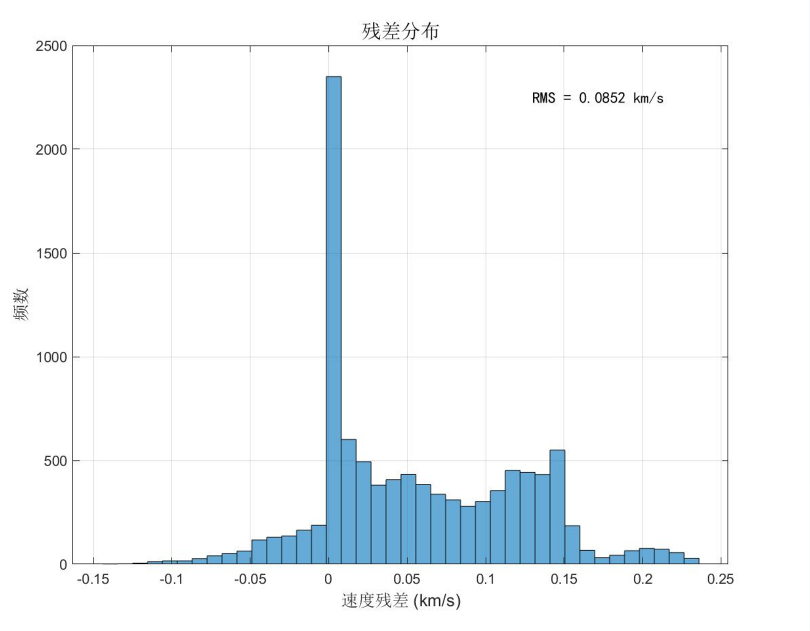

The nearest terrestrial heat flow measurement station to Jinping is about 46.2 km away, with a heat flow value of 50.5 mW/m².

❖ Statistical Characteristics of Terrestrial Heat Flow

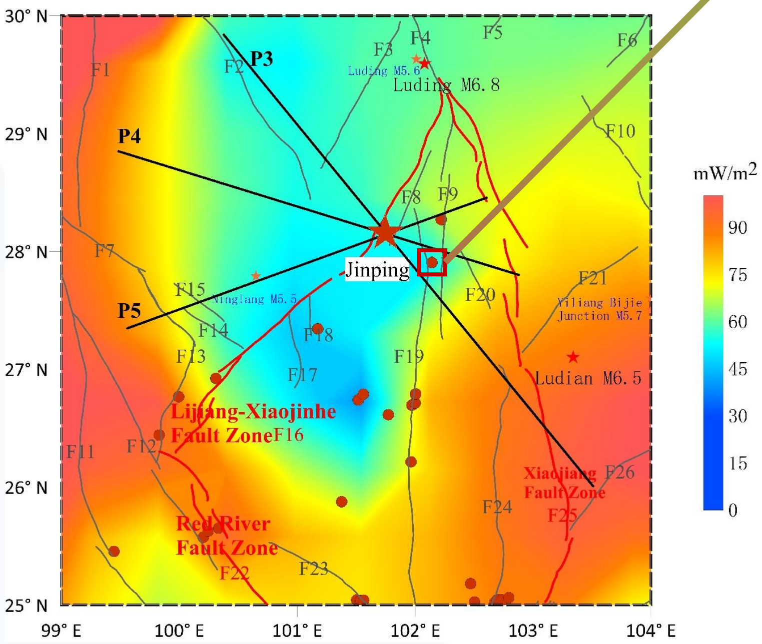

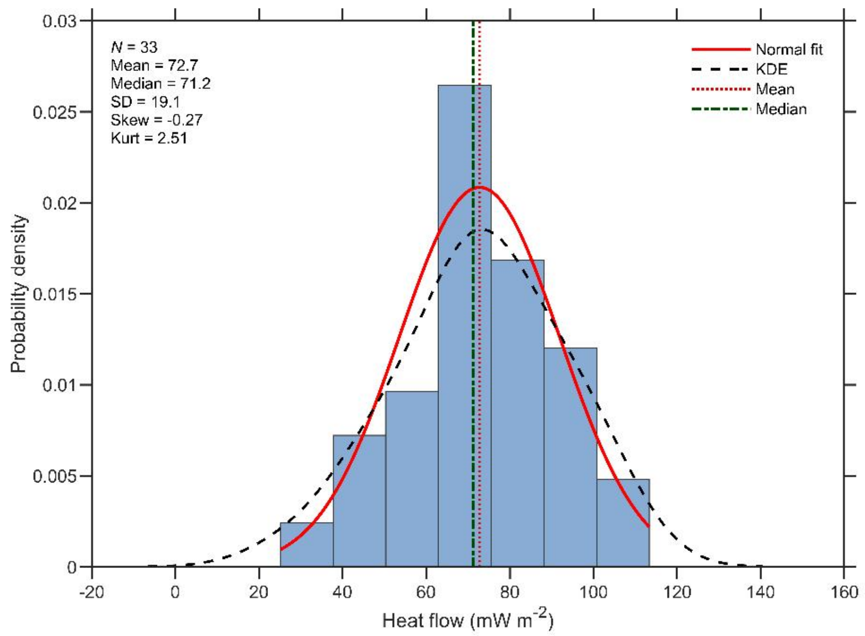

Index	Value	Unit	Description
Sample Size N	33	—	Valid measurement points
Mean	72.7	mW/m2	Regional background heat flow
Median	71.2	mW/m2	Robust central tendency
Minimum (Min)	26.8	mW/m2	Cold thermal anomaly end-member
Maximum (Max)	107.0	mW/m2	Hot thermal anomaly end-member

- **The regional average heat flow of 72.7 mW/m² is generally high, with a wide range of heat flow values.**
- **50% of the heat flow data are concentrated between 66–87 mW/m².Distinct cold and hot thermal anomalies coexist within the study area, while the overall distribution is approximately continuous.**

Results and Discussion

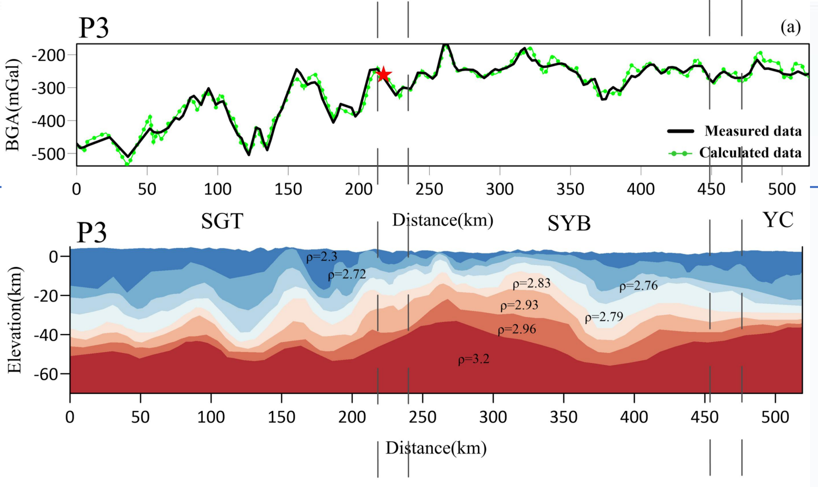

❖ Crustal Temperature (P3)

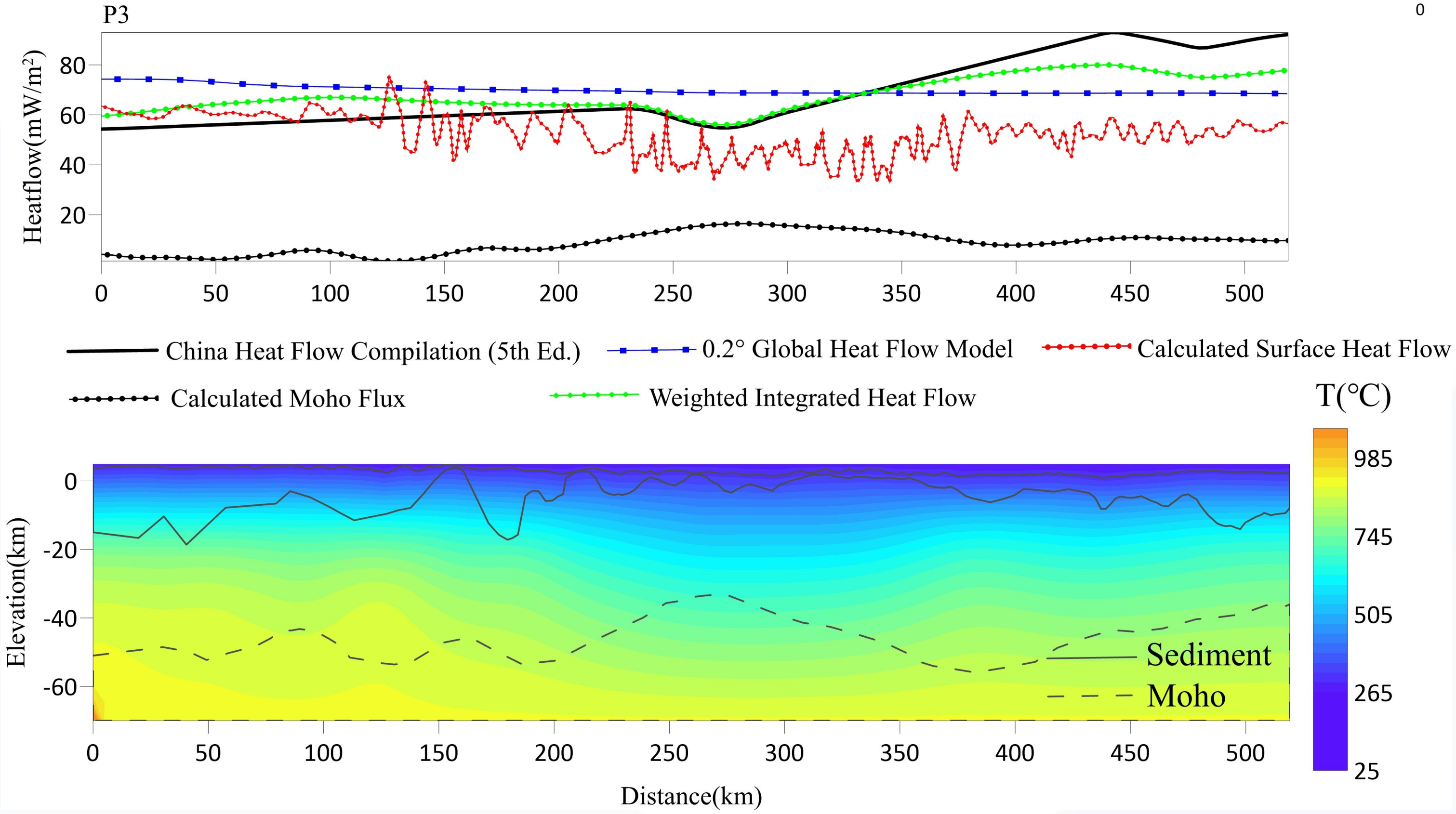

Surface Heat Flow and Crustal Temperature Distribution along Profile P3

➢ Surface Heat Flow Characteristics

- The calculated heat flow is generally lower than the other three surface heat flow curves, and its macroscopic trend is consistent with the 5th Edition Compiled Heat Flow of China.
- The Moho heat flow remains within the low range of 5~20 mW/m² along the whole profile, with a slight uplift in the middle segment.

➢ Deep Temperature Structure

- At identical depths, the temperature in the middle segment of the profile is relatively low, while temperatures on both sides are higher.

Results and Discussion

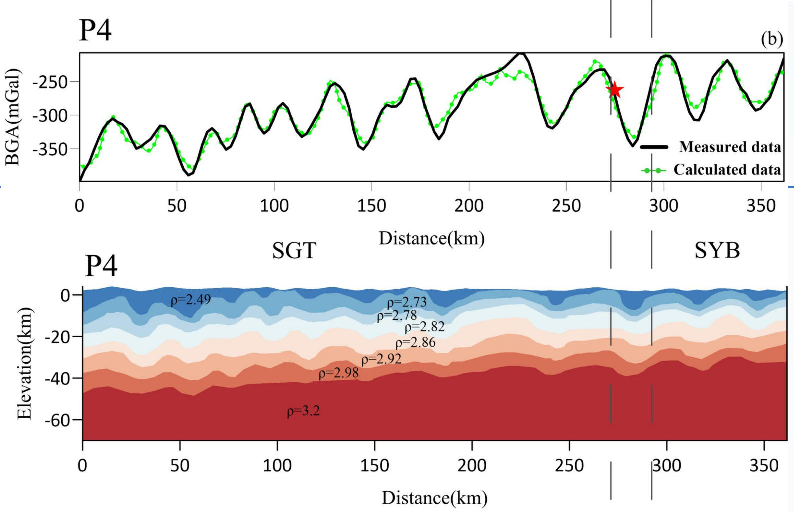

❖ Crustal Temperature (P4)

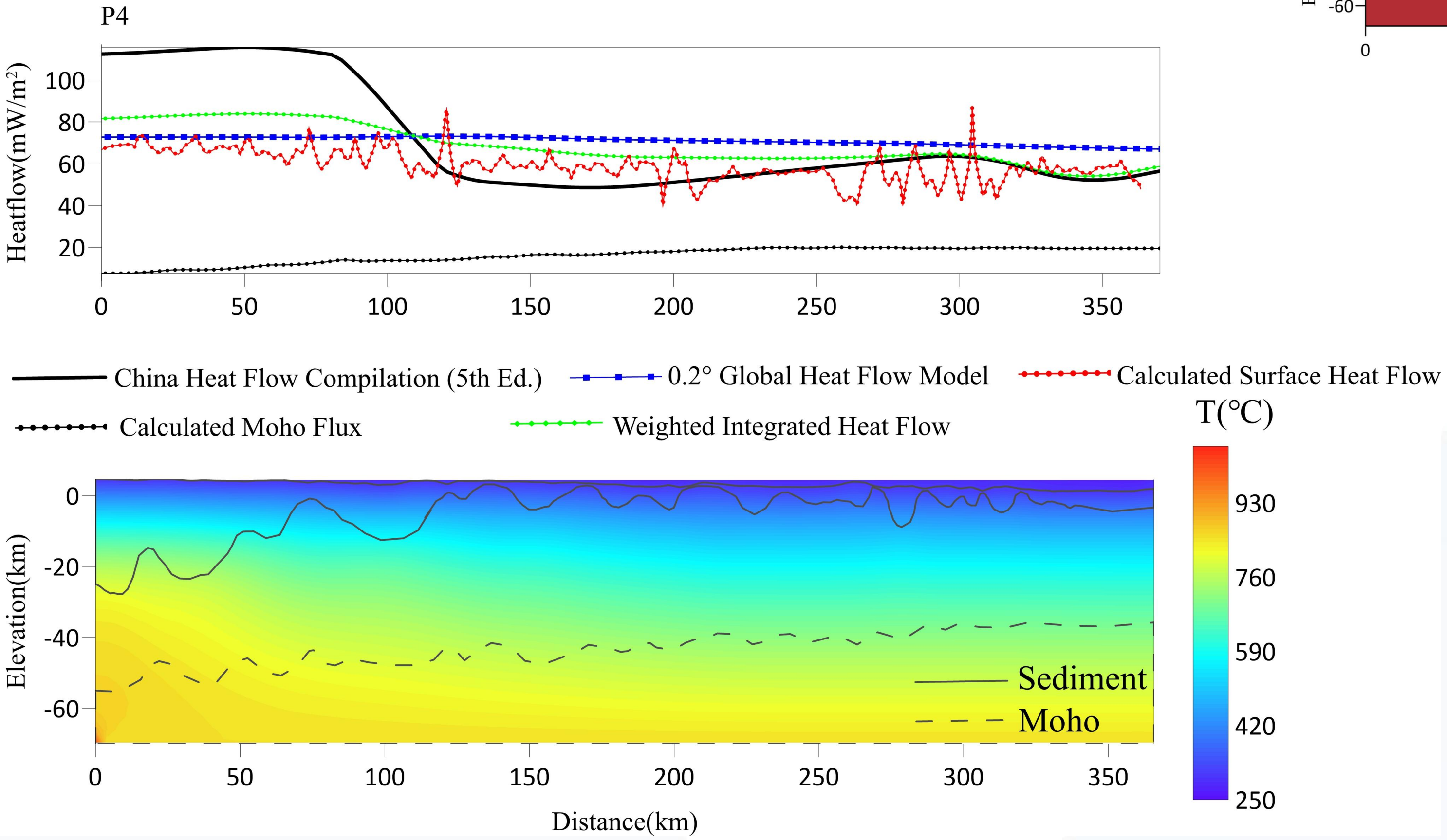

Surface Heat Flow and Crustal Temperature Distribution along Profile P4

➢ Surface Heat Flow Characteristics

- The western measured heat flow shows prominent high anomalies, plummeting 0–100 km and holding moderate-low values (45–60 mW/m²) from 100–360 km; the middle segment is the regional heat flow low. Calculated heat flow is lower than compiled data, reproducing the west-high-east-low pattern. Moho heat flux stays low and rises mildly along the profile.

➢ Deep Temperature Structure

➢ The Moho deepens eastward, with crustal temperatures falling at equal depths, matching the decay of surface heat flow.

Results and Discussion

❖ Crustal Temperature (P5)

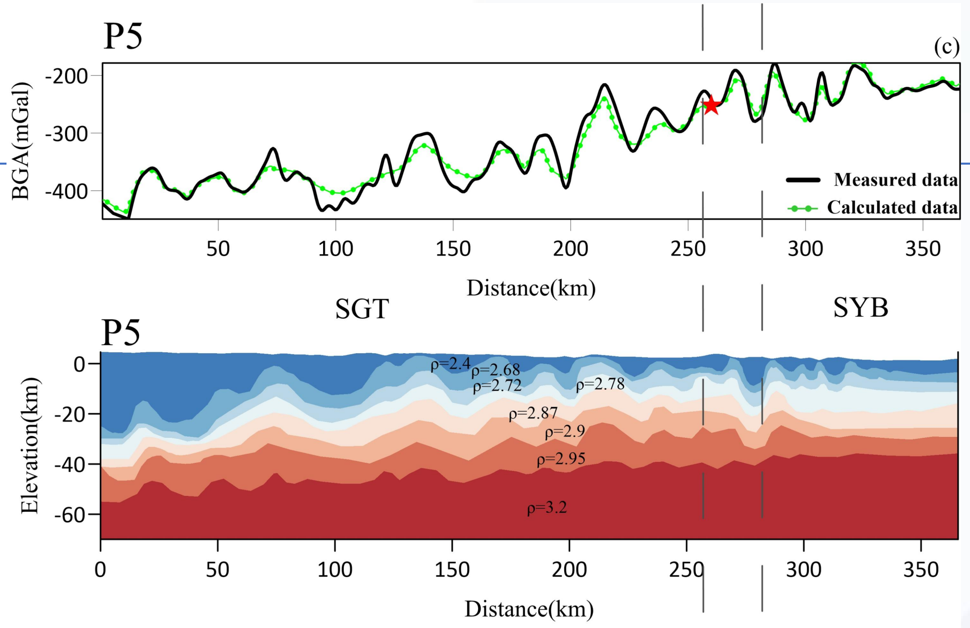

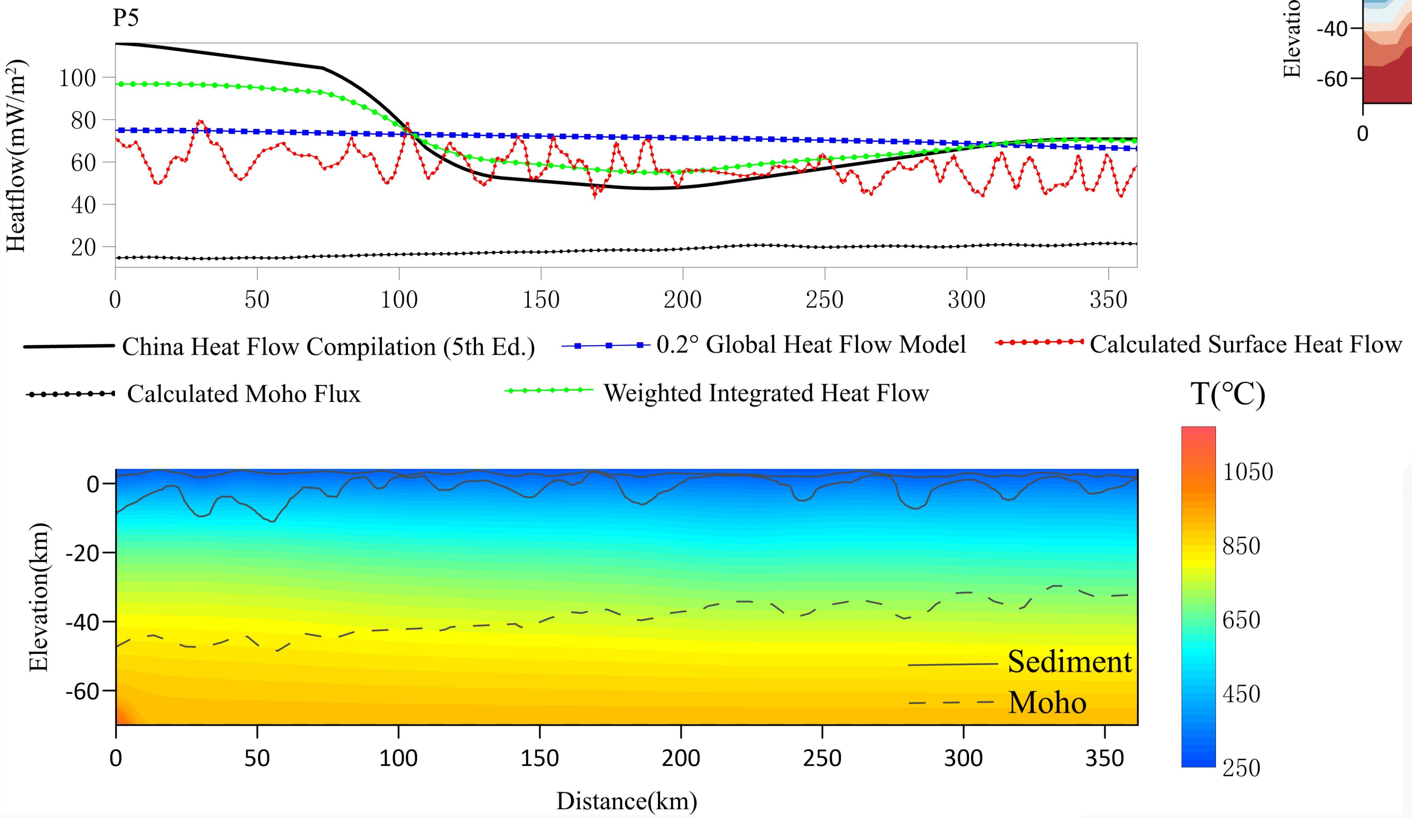

Surface Heat Flow and Crustal Temperature Distribution along Profile P5

➢ Surface Heat Flow Characteristics

- The variation trend of surface heat flow is similar to that of Profile P4.
- Moho heat flux rises gently from west to east, reaching approximately 20 mW/m² east of the middle segment.

➢ Deep Temperature Structure

- The Moho discontinuity gradually deepens eastward, accompanied by a synchronous decrease in deep subsurface temperature.

❖ Research Parameter Table

Calculation Table of Crust-Upper Mantle Radiogenic Heat Production Rate in Sichuan-Yunnan Region				
Layer	Profile	Density (kg/m³)	Heat Production Rate (μW/m³)	Thermal Conductivity (W/(m·k))
Sedimentary Layer	P3	2300	1.43	2.5
	P4	2490	1.56	
	P5	2400	1.57	
Upper Crust 1	P3	2720	1.70	2.55
	P4	2730	1.70	
	P5	2680	1.67	
Upper Crust 2	P3	2760	1.72	2.6
	P4	2780	1.73	
	P5	2720	1.70	
Middle Crust1	P3	2790	1.02	2.65
	P4	2820	1.03	
	P5	2780	1.02	
Middle Crust2	P3	2830	1.04	2.7
	P4	2860	1.05	
	P5	2870	1.05	
Lower Crust 1	P3	2930	0.203 (Sramek et al. ,2016)	3
	P4	2920	0.202 (Sramek et al. ,2016)	
	P5	2900	0.201 (Sramek et al. ,2016)	
Lower Crust 2	P3	2960	0.205 (Sramek et al. ,2016)	3
	P4	2980	0.206 (Sramek et al. ,2016)	
	P5	2950	0.204 (Sramek et al. ,2016)	
Upper Mantle(CLM)	P3/P4/P5	3200	0.027 (Sramek et al. ,2016)	3.2

***Note**: The element abundance data are derived from Sramek et al. (2016);Relevant References:(1) Huang F et al., 2015; (2) Luo F et al., 2024;(3) Huang S D, 2023;(4) Zheng J et al., 2020.*

Prospects

❖ Scientific Significance and Limitations of This Study

- The inversion fitting performs poorly with insufficient accuracy.
- This study mainly relies on model-derived data, while the quantity of in-situ measured terrestrial heat flow data within the research area is insufficient.
- The rock physical property parameters adopted in this research are limited; most parameters are set based on previous empirical values, leading to weak constraint on solution non-uniqueness.

❖ Prospects

- Future research requires integrated interpretation and joint inversion using multiple geophysical techniques and methods.
- More field-measured datasets need to be supplemented, including gravity data and terrestrial heat flow data.

Thank you!

Name: 任雨轩

Email: ryx13293934776@163.com

可乐必胜客

扫一扫上面的二维码图案，加我为朋友。